**GESEP – Gerência de Especialistas em Sistemas Elétricos de Potência**


***Título:***

Operating limits of three-phase multifunctional photovoltaic converters applied for harmonic current compensation.

***Autores:***

V. M. R. de Jesus, L. S. Xavier, A. F. Cupertino, V. F. Mendes and H. A. Pereira**.**

***Publicado em:***

8th International Symposium on Power Electronics for Distributed Generation Systems (PEDG)

***Data da publicação:***

2017

***Citação para a versão publicada:***

V. M. R. de Jesus, L. S. Xavier, A. F. Cupertino, V. F. Mendes and H. A. Pereira, "Operating limits of three-phase multifunctional photovoltaic converters applied for harmonic current compensation," 2017 IEEE 8th International Symposium on Power Electronics for Distributed Generation Systems (PEDG), Florianopolis, 2017, pp. 1-8.

# Operating Limits of Three-Phase Multifunctional Photovoltaic Converters Applied for Harmonic Current Compensation

Victor Magno R. de Jesus[1], Lucas S[1]. Xavier, Allan F. Cupertino[2,3], Victor Flores Mendes[1], Heverton A. Pereira[3]

[1] Graduate Program in Electrical Engineering, Federal University of Minas Gerais,
Av. Antônio Carlos 6627, 31270-901, Belo Horizonte, MG, Brazil
[2] Department of Materials Engineering, Federal Center for Technological Education of Minas Gerais
Av. Amazonas 5253, 30421-169, Belo Horizonte - MG, Brazil
[3] Gerência de Especialistas em Sistemas Elétricos de Potência, Electrical Engineering Department, Federal University of Viçosa
Av. P.H. Rolfs, 36570-900, Viçosa, MG, Brazil

emails: victormagno@ufmg.br, lsantx@gmail.com, allan.cupertino@yahoo.com.br, victormendes@cpdee.ufmg.br, heverton.pereira@ufv.br

***Abstract*— The main objective of a photovoltaic (PV) inverter is to inject the PV power into the ac-grid. Generally, due to variations in solar irradiance, inverters operate bellow their rated current. Therefore, this current margin can be used to ancillary services, such as harmonic current compensation. However, it is necessary to study the photovoltaic inverters voltage and current capability effects during harmonic current injection. In this context, this work presents an algorithm to define the limitations imposed by the dc-link voltage and the inverter current. The algorithm is validated through a simulation and an overview of the simulation characteristics are also presented in this paper. Simulation results show that the algorithm can well estimate the amount of current that can be synthesized by the converter. According to the results, it is demonstrated that the dc-link voltage, the characteristics of the filter and the harmonic order contribute to the amount of harmonic current that can be synthesized by the converter.**

***Keywords—harmonic compensation; multifunctional converter; operating limits; photovoltaic systems.***

## I. INTRODUCTION

Several studies have proposed the operation of multifunctional photovoltaic inverters that operate in the power system with auxiliary services, adding functions to compensate harmonic currents and / or providing reactive power [1]-[3]. Among the harmonic detection methods used in the literature, the method of instantaneous power theory (IPT) proposed by [4] is strongly recommended. This method allows to separate the power components related to each type of disturbance into three orthogonal components, active, reactive and harmonic component. Thus, it is possible to generate the reference current required to perform the compensation.

Several papers propose different techniques for harmonic compensation using control structures. For example, proportional-integral (PI), proposed by [5], - [7]. Furthermore, the resonant control (PR) is also employed, as proposed by [4], [8] and [9].

Additionally, according to [10] the inverter switches have a current limit that cannot be exceeded. The inverter current reference is composed by active and harmonics components. To avoid injection of low order harmonics in the grid, the current reference needs to be dynamically saturated. Therefore, techniques for partial compensation for load harmonic currents are required. It is proposed in [11] a dynamic saturation scheme which measures the harmonic components according to the rated peak current value of the inverter.

It is worth mentioning that the main function of photovoltaic inverters is to provide active power for the grid. With this in mind, studies of the effects of harmonic compensation on the efficiency of photovoltaic inverters are needed. The focus of this paper is to determine the voltage and current capability of the converter with an LCL filter, and the constraints caused by this element during harmonic compensation. Since the filter is generally designed to restraint the harmonic injection into the grid, it may influence the capacity of the inverter to synthesize the required harmonic. It is important to understand the variables that can somehow limit the harmonic compensation.

In this work is presented an algorithm to define the limitations imposed by the dc-link voltage and the inverter current. The algorithm is validated through a simulation at MATLAB/Simulink. An overview of the characteristics presented in the simulation are also presented in this paper.

## II. SYSTEM STRUCTURE

A three-phase photovoltaic inverter is analyzed in this work. It is a 10 kW, with an LCL filter connected to the power grid, as depicted in Fig. 1. As we are interested in the effects in the grid side, the solar panel side was represented in a simplified way, without the dc-dc stage

The system uses an IGBT bridge to transform the dc current of the PV panels in alternated current. An LCL filter connects the converter to the grid in order to mitigate the switching frequency harmonics.

**978-1-5090-5339-1/17/$31.00 ©2017 IEEE.**

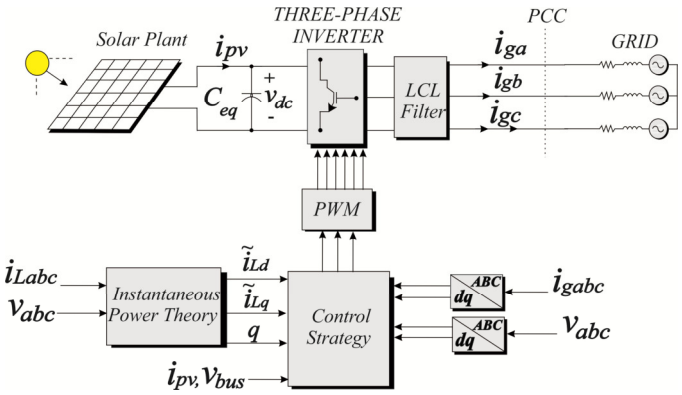


Figure 1. Topology of the system.

## III. CONTROL STRUCTURE

The Complete control structure is shown in Fig. 2. The control strategy is based on the grid side current measurement and the dc-link voltage control is based on the voltage-squared control method.

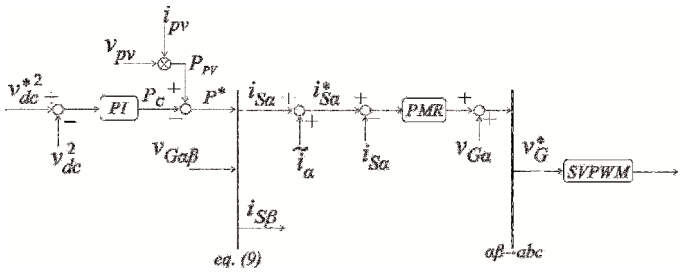


Figure 2. Complete control structure.

### A. Outer-Loop Control

The outer loop controls the voltage at the dc-link, and it is based on the energy stored in the capacitor. Where,

$$W = \frac{1}{2} C_{eq} v_{dc}^2 . \tag{1}$$

Considering the time derivative of (1) equal the instantaneous capacitor power, in frequency domain:

$$P_{cap}(s) = P_{PV}(s) - P_{IN}(s) = \frac{1}{2} C_{eq} v_{dc}^2 s . \tag{2}$$

Thus, considering $P_{PV}$ (power supplied by the PV plant) as a feedforward term, a linear relation between the injected power $P_{cap}(s)$ and squared dc-link voltage is obtained. In the outer loop controller design, PI(s), the inner loop is regarded ideal. Thus, the closed-loop transfer function is obtained:

$$G_{cl}(s) = \frac{2k_p(\tau_i s + 1)}{\tau_i C_{eq} s^2 + 2k_p(\tau_i s + 1)} \tag{3}$$

Where $k_p$ and $\tau_i$ are PI controller parameters. Two poles are allocated at frequencies $w_{c2}$ and $w_{c3}$. Thus, the outer loop controller gains can be calculated by:

$$\omega_{c2} + \omega_{c3} = \frac{2k_p}{C_{eq}} \Rightarrow k_p = \frac{C_{eq}(\omega_{c2} + \omega_{c3})}{2} \tag{4}$$

$$\omega_{c2} * \omega_{c3} = \frac{2k_p}{C_{eq}\tau_i} \Rightarrow k_{i2} = \frac{C_{eq}(\omega_{c2} * \omega_{c3})}{2} . \tag{5}$$

### B. Inner Loop control

If balanced grid conditions are assumed, one can obtain the following relation:

$$v_{sj} = Ri_{sj} + L\frac{di_{sj}}{dt} + v_{gj} \tag{6}$$

where $v_{si}$ and $v_{gj}$ represent the converter alternating terminal voltage and the grid voltage of phase $j = a,b,c$, respectively, and $i_{gj}$ represents the output converter current. R and L represent the filter resistance and inductance, respectively. Equation (6) can be written in the stationary reference frame, as given by:

$$v_{s\alpha} = Ri_{s\alpha} + L\frac{di_{s\alpha}}{dt} + v_{g\alpha} \tag{7}$$

$$v_{s\beta} = Ri_{s\beta} + L\frac{di_{s\beta}}{dt} + v_{g\beta} . \tag{8}$$

The inner loop controls the current injected into the power system, the control uses the reference obtained from the IPT theory as well the harmonic current, provided by the instantaneous power theory. The IPT consists of separating a current signal in three orthogonal components: active, reactive and harmonic component. The currents are obtained by the following equations [4]:

$$\begin{bmatrix} i_\alpha \\ i_\beta \end{bmatrix} = \frac{1}{v^2{}_\alpha + v^2{}_\beta} \begin{bmatrix} v_\alpha & v_\beta \\ v_\beta & -v_\alpha \end{bmatrix} \begin{bmatrix} p \\ q \end{bmatrix} . \tag{9}$$

In order to compensate harmonics, the signal obtained with (9) is separated using a high pass filter, the oscillating components $\tilde{p}$ and $\tilde{q}$ are separated from the continuous components $\bar{p}$ and $\bar{q}$. Harmonic detection based on IPT is presented in the block diagram of Fig. 3. More details about this theory are shown in [4]. Thus, the fundamental components of the current are combined with the oscillating components $i_{\alpha\beta}$, generating the inverter current reference $i^*_{S\alpha\beta}$.

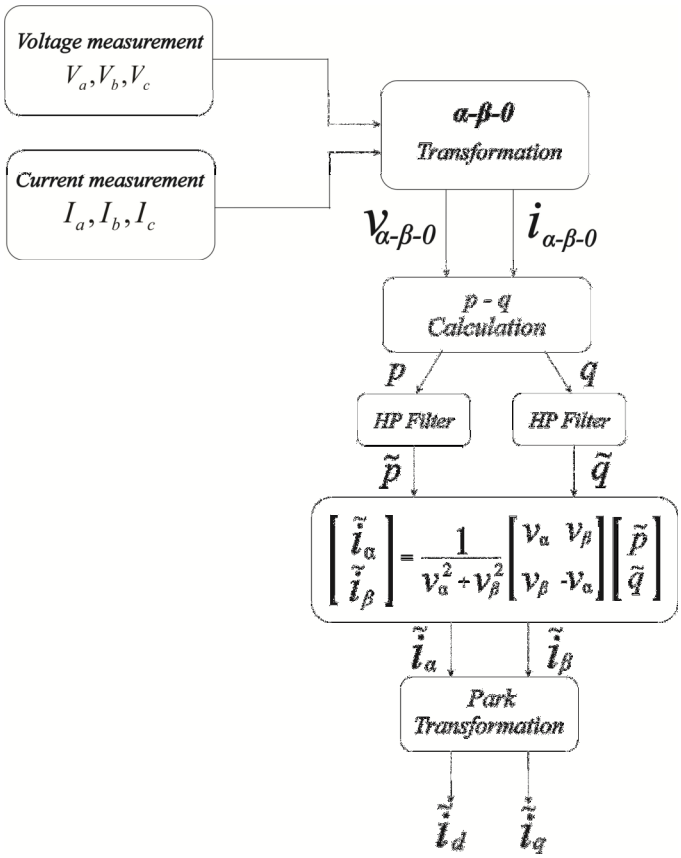


Figure 3. Harmonic detection method.

The PMR controller tunning considers the crossover frequency of the controller and its relationship with the critical point in the Nyquist diagram, as proposed in [7]. PMR controller is based on proportional and multiples resonant controllers. It can be expressed in the s-domain as:

$$G(s) = K_p + \sum_h K_{Ih} \frac{s}{s^2 + h^2 \omega_n^2} \tag{10}$$

Where $K_p$ is the proportional gain and $K_{Ih}$ is the resonant gain of each parcel. The last term of (10) consists in resonant controllers for tracking harmonics of order $h$ ($\omega_1$ is the fundamental frequency). Implementing this controller in αβ-reference frame, each resonant controller can compensate only one harmonic order. The resonant compensators must be carefully adjusted, since some harmonics can be found above the crossover frequency of the current loop, leading to instabilities. These instabilities can be identified by the means of Nyquist diagram as proposed in [7].

## IV. Operating Limits

### A. Dc-link voltage limit

It is depicted in the Fig. 4 one of the phases of the LCL filter. $V_s$ is the converter synthesized voltage and $V_g$ is the grid voltage.

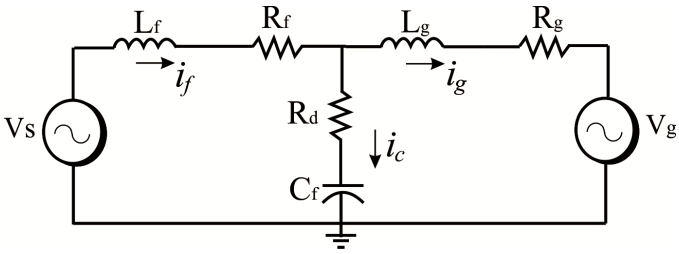


Figure 4. LCL filter model.

The phasor diagrams of the voltages and currents of the presented circuit is represented in Fig. 5, where $\theta$ is the angle between the point of common coupling and the injected current, and the voltages are given according to LCL filter reactance.

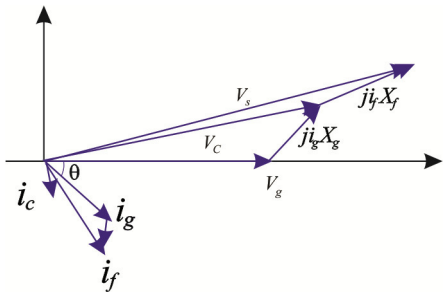


Figure 5. Phasor diagram.

It is necessary to obtain the voltage synthesized by the converter as a function of the current flowing to the grid. Then it is possible to extract the following equations from the circuit,

$$V_c = V_g + jX_g I_g \tag{11}$$

$$I_c = \frac{V_c}{-jX_c} \tag{12}$$

$$V_s = V_c + \left(I_c + I_g\right) X_f \tag{13}$$

In this way, the equation relating the required synthesized voltage to flow for a given current is obtained. It is worth mentioning that the equation above is also valid for harmonic currents, only by disregarding the grid voltage term of (11).

Regarding the second part of the problem, the dc-link needs a minimum value in order to provide the power injection in the grid. This minimum value guarantees that the modulation will occur in the linear region and, therefore, no low frequency harmonics will be generated.

For the system simulated in this work the required dc-link voltage can be calculated as follow. A PWM modulation (Third Harmonic injection PWM) is used, where the modulation index of the technique for the linear operation is m = 1.1547 [14], the equation that relate the modulation index, the grid voltage and the dc-link is (14),

$$m = \frac{2\hat{V}_g}{V_{dc}} \tag{14}$$

Thus, by (14) the minimum voltage of the dc-link must be at least:

$$V_{dc} = \frac{2\hat{V}_g}{1,1547} = 1,732\hat{V}_g \approx \sqrt{3}\hat{V}_g \tag{15}$$

Using (14), it is implemented an iterative algorithm that searches for the maximum harmonic current that can be synthesized by the converter without exceeding the voltage limits of the dc-link.

As input information, the power flowing through the grid, the dc-link voltage, the harmonic order and the filter characteristics must be provided.

The first step is to calculate by (11), (12) and (13) the necessary dc-link voltage to flow the specified active power to the grid. Then, the harmonic current values are iterated. For each angle value of the harmonic to be synthesized, an iteration is made by increasing the module of the current until the stop condition is satisfied. In this case, the stop condition is the voltage value of the dc-link divided by $\sqrt{3}$.

The algorithm then returns the maximum harmonic current values that can be synthesized by the converter without exceeding the DC bus voltage constraint. Fig 6 present the flowchart diagram for the algorithm. $V_1$ and $V_h$ are the dc-link voltage required for the fundamental current and the harmonic current, respectively. The $h$ value identify the harmonic order of the compensated current, $I_h$ and $\delta_h$ are the module and angle of the harmonic current to be compensated.

### B. *Converter current limit*

The current limits, although straightforward to investigate, are also important for the correct functioning of the converter. In this case, the vectorial sum of the fundamental current flowing into the grid with the harmonic current to be synthesized cannot be greater than the rated current of the converter. In practice a service factor of 10% is used and will also be adopted in this work.

It is important to note that the angle at which the harmonic occurs influences in the amount of harmonic current that can be injected into the grid. In some cases the peak of the resulting waveform decreases. Fig. 7 exemplifies for a fictitious case this occurrence.

In this case, a third harmonic current with module equal to 5.17 A was added to a fundamental (60 Hz) waveform with module 15.5 A and 90º phase angle. In the first graph the third harmonic current has a 270º phase angle, the sum, results in a waveform with a 20.66 A peak value.

In the second graph, the third harmonic current has a phase angle of 180º resulting in a peak value of 14.61 A.

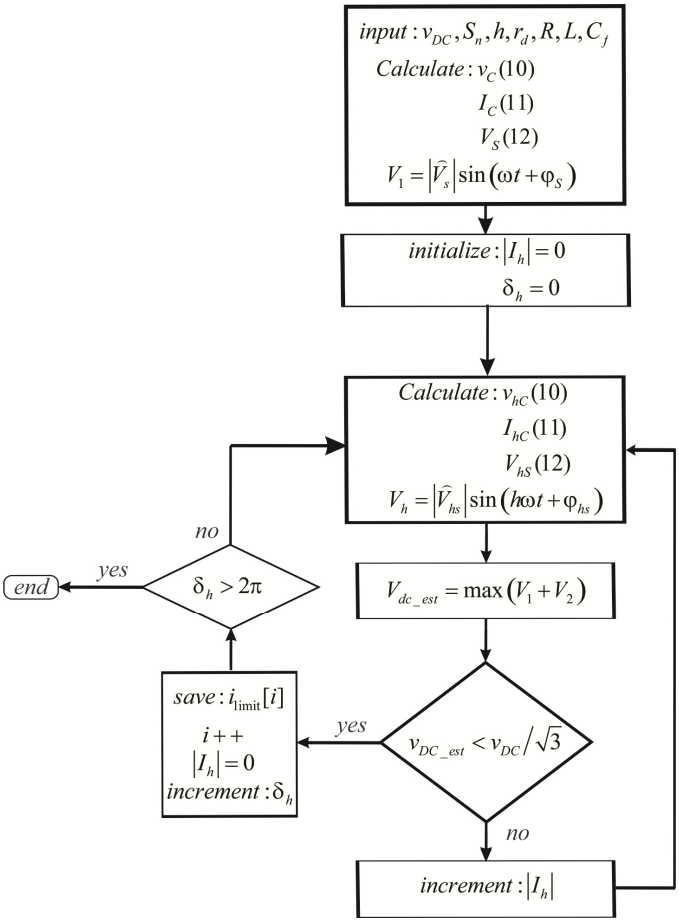


Figure 6. Flowchart diagram of the algorithm.

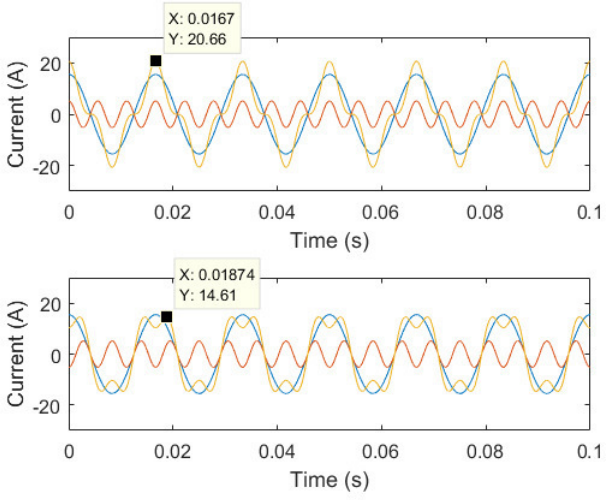


Figure 7. Exemplification of different angles in the harmonic current.

## V. System Simulation and Results

The system presented in Section II with the control structure described in Section III was simulated using MATLAB/Simulink© in order to evaluate the capability of the proposed algorithm to identify voltage and current limits.

TABLE I. System Parameters

| Parameters | Value |
|---|---|
| Grid Voltage | 380 V |
| Grid frequency | 60 Hz |
| Inverter rated power | 10 kW |
| Swicthing frequency | 12 Khz |
| Filters capacitance | 3.8 uF |
| Filters inductances | 1 mH |
| Filters resistances | 0.01 Ω |
| Damping resistor | 22.94 Ω |

### A. *Validation of the algorithm*

Firstly, the algorithm response is analyzed under rated power flowing to the grid and a dc-link voltage of 570 V.

The simulations limitation is obtained measuring the maximum amplitude of the reference signal. Fig. 8 shows the simulation and the algorithms results for harmonic current limits. The figure is represented in polar diagram, with the units presented in per-unit (p.u.), with the base current equals the rated current of the converter. In the polar diagram the module and angle represents the amplitude and the phase angle of the harmonic current, respectively.

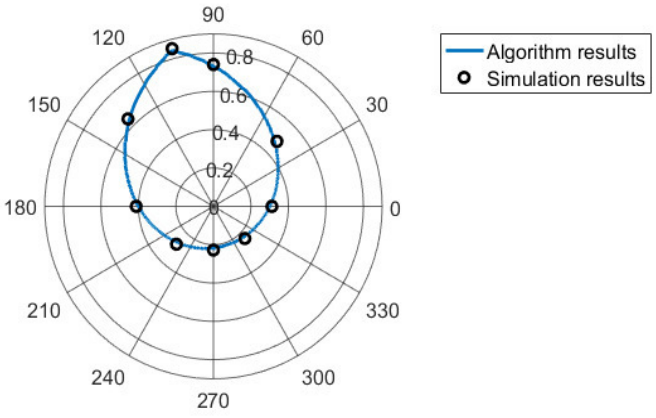


Figure 8. Harmonic injection limit with a dc-link voltage of 570 V.

Fig. 9 presents the synthetized voltage of the simulation and the estimation obtained by the algorithm. For this simulation, a fifth harmonic current of 6 A is used with a 0º phase angle.

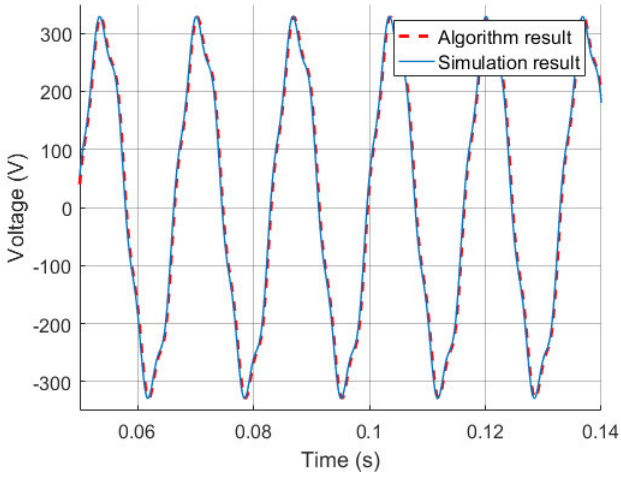


Figure 9. Voltage reference synthesize by the the inverter .

In Fig. 10 are presented the synthetized voltage of the simulation and the estimation obtained by the algorithm. For this simulation, a fifth harmonic of 3 A was add to a seventh harmonic current of 2 A, for both current the phase angle used was 0º.

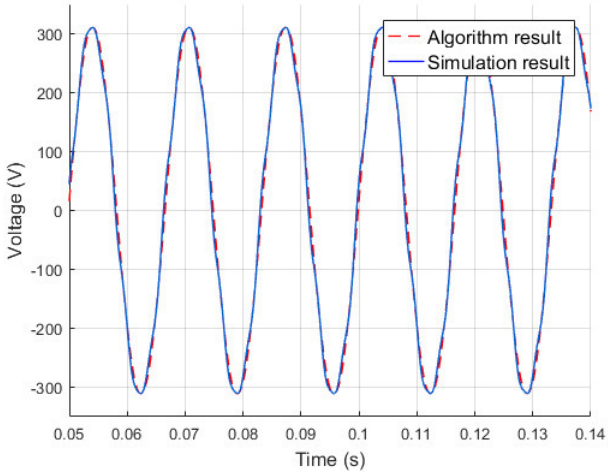


Figure 10. Voltage reference for the inverter to synthesize.

Fig. 11 shows the simulation and the algorithms results for harmonic current limits considering the converter current limit. Fig. 11 is represented in polar diagram, with the units presented in per-unit (p.u.), with the base current equals the rated current of the converter. In the polar diagram the module and angle represents the amplitude and the phase angle of the harmonic current, respectively.

The algorithm can estimate the necessary dc-link voltage in order to provide the required harmonic current, it can also estimate the converter current limit. With that in mind, we can go further in the investigations of the factor that influences in the capacity to inject harmonics currents.

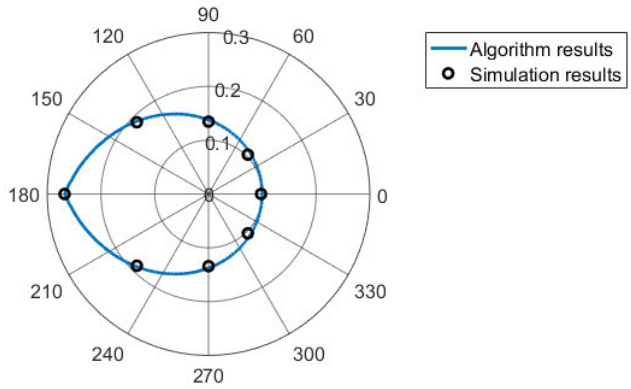


Figure 11. Current injection limit.

### B. *Dc-link voltage*

Now, a variation in the dc-link voltage will be analyzed. It starts with 545 V, a little more that the required voltage to inject the rated power into the grid. Also, the current limit of the converter it is shown. The presented result is for a fifth harmonic current with a 0º phase angle. Once again, the results in Fig. 12 are shown in p.u.

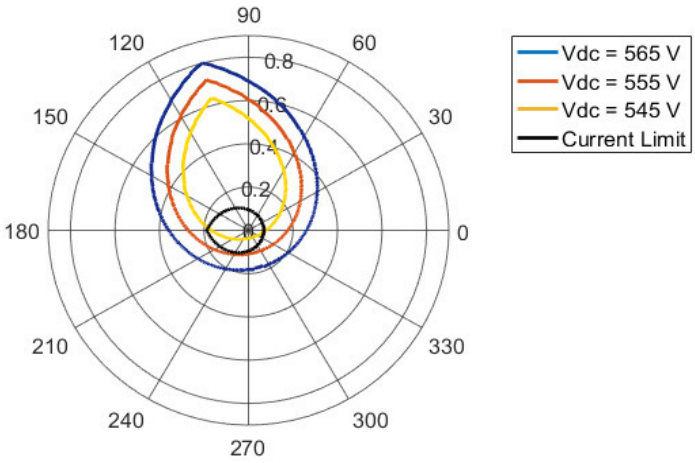


Figure 12. Dc-link variation influence in the harmonics injection limits.

As can be seen, with an increase in the dc-link voltage the limit of harmonic injection increases, mostly due to different voltages drop for different harmonics frequencies. With 545 V in the dc-link, the intersection between the converter current limits and the dc-link voltage limit gives the operating limits of the PV system for this condition. Nonetheless, for higher voltages at the link-dc, the current limit is solely responsible for the limit of operation.

### C. *Harmonic order*

Due to the distinct impedance of the LCL filter for each different harmonic order, it is expected that amount of current for each harmonic order will vary. In this case a 570 V dc-link will be used and the inverter with rated power flowing to the grid. Fig 13, represented in polar diagram, presents the results for four harmonics order.

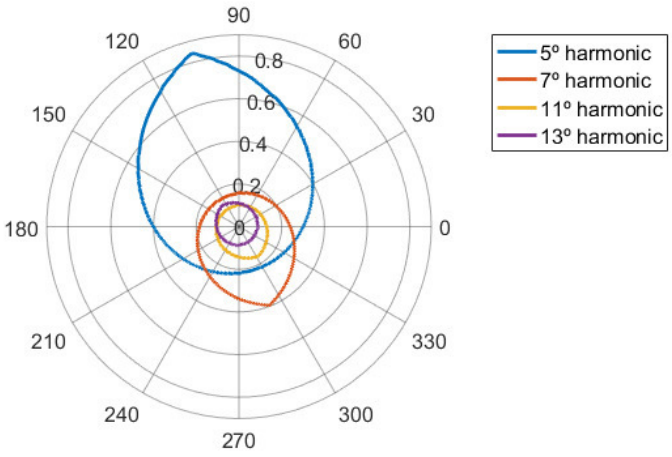


Figure 13. Different limits per harmonic order.

One can notice that the limit differs not only in the module, but also the angle where the maximum current limitation occurs. Focusing on the amount of harmonic current that can be synthesize by the converter, Fig. 14 shows a 3-D graph where is presented the maximum harmonic current depending on the harmonic order and the dc-link voltage.

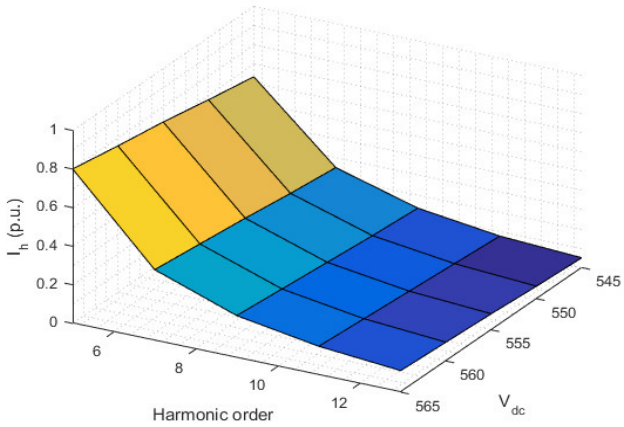


Figure 14.

It can be seen the direct influence of the dc-link voltage, as well the harmonic order in the amount of harmonic current that can be synthesized by the inverter.

### D. *Converter capability*

Until now, in all the cases analyzed, the converter is injecting rated power into the grid. It is valid to remember that the photovoltaic converter will not operate at full capacity during all the day. For the last case, it will be realized a comparison when the capacity of the converter is fully available against the condition with rated power. A 570 V dc-link is used for this case. Fig. 15 shows the results.

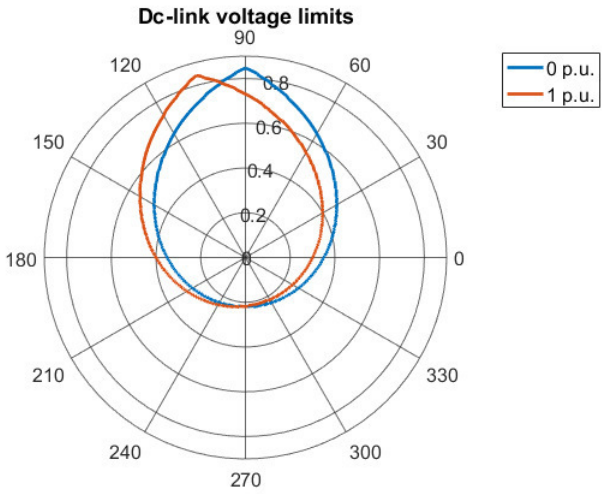


Figure 15. Comparison between system at full capacity and with zero power flowing to the grid.

As can be seen, the differences are not substantial, but the maximum point is dislocated due to the different contribution of the fundamental current in those cases. This can be explained, over the necessity of parallelism with the ac grid in order to provide the harmonic current to the grid. Even with no active power flowing to the grid, the converter must synthesize a reference compatible with the grid voltage.

For comparison purposes, the same analysis will be done for the current limits. Fig. 16 shows the comparison between the system at different active power levels.

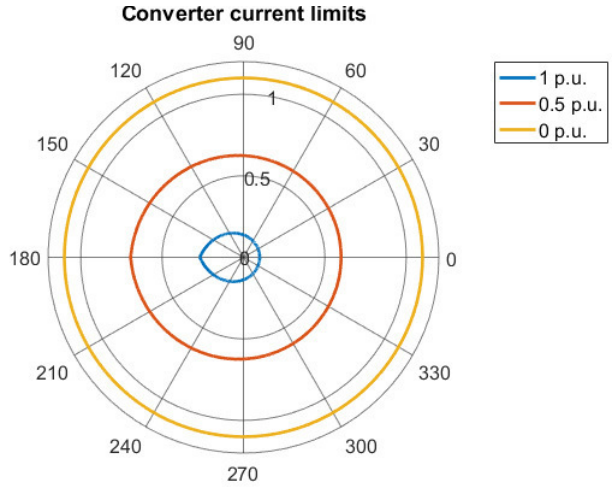


Figure 16. Comparison between system at full capacity, half capacity and with zero power flowing to the grid.

In this case, the system capacity greatly influences the harmonics current limits, as expected. Since the peak value of the resulted current is what matters, 1 p.u. of fundamental current or 1 p.u. of harmonic current lead to the same value of current peak.

## VI. Conclusions

This work presented an algorithm to estimate the amount of harmonic current that can be synthesized by a PV converter, given the system characteristics as, dc-link voltage, filter configuration and harmonics current order. The algorithm consists in calculate the voltage drop in the filter and estimate the voltage reference necessary to flow the harmonic current to the grid.

Results shown that the algorithm can estimate with a high precision the needed voltage in the dc-link in order to provide the required harmonic current. With an increase in the dc-link voltage the limit of harmonic current injected increases.

The harmonic order influences in the limitation due to the filters characteristics, higher the frequency higher the voltage drop across the filter elements. The available capacity of the converter does not cause a substantial alteration in the harmonic current limit due to dc-link voltage, but the maximum point is dislocated due to the different contribution of the fundamental current in those cases.

For future work, the authors are working on a prototype to test and compare the algorithm with experimental results and different levels of harmonic currents conditions.

## Acknowledgment

This work has been supported by the Brazilian agency CAPES. The authors would like to thanks CNPQ, FAPEMIG and CAPES for their assistance and financial support.

## References

[1] Bonaldo, J. P.; Pomilio, J. A. Multi - Functional Use of Single-Phase Power. IEEE PES Innovative Smart Grid Technology Conference, São Paulo, April 2013.

[2] Munir S., Li Y. W., “Residual Distribution System Harmonic Compensation Using PV Interfacing Inverter”, IEEE Transaction on Smart Grid, vol. 4, no. 2, pp. 816-827, June 2013.

[3] L. Xavier, A. Cupertino and H. Pereira, “Adaptive saturation scheme for a multifunctional single-phase photovoltaic inverter,” Industry Applications (INDUSCON), 2014 11th IEEE/IAS International Conference on, pp. 1-8, 7-10 Dec. 2014.

[4] H. Akagi, E. Watanabe and M. Aredes, “Instantaneous Power Theory and Applications to Power Conditioning,” vol. 1, Wiley-IEEE Press, 2007, pp. 109 - 220.

[5] J. Miret, M. Castilla, J. Matas, J. Guerrero and J. Vasquez, “Selective Harmonic-Compensation Control for Single-Phase Active Power Filter With High Harmonic Rejection,” Industrial Electronics, IEEE Transactions on, vol. 56, no. 8, pp. 3117-3127, Aug. 2009.

[6] Kalaignan T. And Raja T., “Harmonic elimination by Shunt active filter using PI controller,” Computational Intelligence and Computing Research (ICCIC), 2010 IEEE International Conference on, pp. 1-5, Dec. 2010.

[7] A. Yepes, F. Freijedo, O. Lopez and J. Doval-Gandoy, “Analysis and Design of Resonant Current Controllers for Voltage-Source Converters by Means of Nyquist Diagrams and Sensitivity Function,” Industrial Electronics, IEEE Transactions on , vol. 58, no. 11, pp. 5231-5250, Nov. 2011.

[8] Bojoi, R. I. et al. Current Control Strategy for Power Conditioners Using Sinusoidal Signal Integrators in Synchronous Reference Frame. IEEE TRANSACTIONS ON POWER ELECTRONICS, NOVEMBER 2005. 1402 - 1412.

[9] C. Lascu, L. Asiminoaei, I. Boldea and F. Blaabjerg, “High Performance Current Controller for Selective Harmonic Compensation in Active Power Filters,” Power Electronics, IEEE Transactions on, vol. 22, no. 5, pp. 1826-1835, Sept. 2007.

[10] T. Qian, B. Lehman, G. Escobar, H. Ginn and M. Molen, “Adaptive saturation scheme to limit the capacity of a shunt active power filter,” Control Applications, 2005. CCA 2005. Proceedings of 2005 IEEE Conference on, pp. 1674-1679, 28-31 Aug. 2005.

[11] Ramon M. D., Xavier L., A. Cupertino, H. Pereira, “Current Control Strategy for Reactive and Harmonic Compensation with Dynamic Saturation”.

[12] Rodrigues V. M. De Jesus, Cupertino A., Xavier L., Mendes V. F. And Pereira H., “Comparison of MPPT Strategies Applied in Three-Phase Photovoltaic Inverters during Harmonic Current Compesation” Industry Applications (INDUSCON), 2016 12th IEEE/IAS International Conference on, Nov. 2016.

[13] Liserre M., Dell’aquila A., And Blaabjerg F., “Stability improvements of an LCL-filter based three-phase active rectifier,” 2002 IEEE 33rd Annu. IEEE Power Electron. Spec. Conf. Proc. (Cat. No.02CH37289), vol. 3, pp. 1195–1201, 2002.

[14] Bin Wu, "High-Power Converters and AC Drives," IEEE Press/Wiley-Interscience, 2006.